LOCAL YIELDING AND EXTENSION OF A CRACK UNDER PLANE STRESS†

G. T. HAHN and A. R. ROSENFIELD‡

The size of locally yielded regions, the stress distribution, and displacements attending a crack in tension under plane stress have been calculated by extending the work of Dugdale and others. Methods have been developed to take work-hardening and unloading into account. The displacements and plastic-zone sizes measured in edge-slotted silicon steel coupons are found to be in agreement with calculations. Conditions under which plane stress or plane strain are dominant in these edge-slotted specimens have also been determined. Finally, Irwin's fracture-toughness parameter and the conditions for crack extension are formulated in terms of basic material parameters consistent with experiment.

DEFORMATIONS PLASTIQUES LOCALES ET EXTENSION D'UNE FISSURE EN ETAT PLAN DE CONTRAINTES

Les auteurs ont calculé, en prolongeant les calculs de Dugdale et d'autres chercheurs, la dimension des zones ayant subi une déformation plastique localisée, la distribution des contraintes et les déformations dans le voisinage d'une fissure sous tension en état plan de contraintes. Ils ont développé une méthode de calcul permettant de tenir compte de la consolidation et de l'effet de déchargement. Les déplacements et les zones déformées plastiquement relevés dans une éprouvette d'acier au silicium entaillée, ont été trouvés en accord avec les résultats du calcul. Les auteurs ont également déterminé dans quelles conditions l'état plan de contraintes ou l'état plan de déformation domine dans une éprouvette entaillée. Finalement, le paramètre proposé par Irwin pour chiffrer l'aptitude d'un métal à résister à la propagation d'une rupture, et les conditions d'extension d'une fissure sont exprimées en fonction des paramètres basiques du matériau qu'on peut tirer de l'expérience.

LOKALES FLIEßEN UND AUSDEHNUNG EINES RISSES BEI EBENER SPANNUNG

Durch Ausdehnung der Arbeit von Dugdale u.a. wurden die Größe lokaler Fließgebiete, die Spannungs-verteilung und die mit einem Riss unter Last bei ebener Spannung verbundenen Verschiebungen berechnet. Es wurden Methoden entwickelt zur Berücksichtigung von Verfestigung und Entlasten. Die an spaltförmig geschlitzten Silizium-Stahl-Proben gemessenen Verschiebungen und Ausdehnungen der plastischen Zonen stimmten mit den Rechnungen überein. Es wurden ferner die Bedingungen bestimmt, unter denen in Proben dieser Art ebene Spannung oder ebene Verzerrung vorherrschend ist. Schließlich werden Irwins Parameter für die Bruchstärke und die Bedingungen für die Rissaus-dehnung durch fundamentale Stoffparameter in Übereinstimmung mit dem Experiment ausgedrückt.

INTRODUCTION

Progress in understanding fracture has been handicapped by the fragmentary picture of stress and strain in front of a crack. Experimental measurements have proven difficult. The elastic-stress-field solutions of Inglis[1] or Irwin[2] are not valid close to and within the very important yielded region generated at the crack tip. The Irwin[2] and Wells[3] treatment, which does take yielding into account, is a reasonable approximation only when the yielded region is small relative to the crack length. At the same time, the quasi-rigorous solutions of elastic–plastic behavior[4-6] are complex and unwieldy; so far, practically no information on the stress and strain within the yielded zone attending a crack in tension has been developed in this way. Thus, it may be useful to compromise some rigor for a simpler tractable approach, particularly to deal with added complications, such as work hardening and rate-sensitive flow. For example, Hult and McClintock's[7] solution for a notch subjected to torsion, a case which is easier to treat, has shed useful light on the situation in tension.[8,9]

Knott and Cottrell[10] were able to exploit the idealized slip band model of a crack under pure shear. developed by Bilby et al.[11] in their study of notched bend specimens.

This paper extends the model of a crack in tension under plane stress developed by Dugdale.[12] and compares its predictions with experimental results. The model, based on a mathematical development of Muskhelishvili,[13] embodies the following assumptions:

(1) The material outside the plastic zone is elastic.

(2) The material within the zone is rigid-perfectly plastic,

(3) A Tresca yield criterion is obeyed,

(4) Yielding is confined to a narrow wedge-shaped zone.§

Dugdale demonstrated that the plastic-zone size predicted in this way is consistent with the behavior of mild steel. Goodier and Field[14] used the model to calculate crack-tip displacements. Results of further work described in this paper show that silicon steel—even in the form of reasonably thick plates —can exhibit a zone similar to that prescribed by

§ This may be a consequence of the Tresca criterion.

the DM (Dugdale–Muskhelishvili) model. Measurements of plastic-zone size and the crack-tip displacement both on-load and after unloading are shown to be in accord with theory. The results also provide insight into the mechanism and conditions favoring the DM zone. The stress gradient in front of the plastic zone is calculated and methods of treating work-hardening and unloading are explored. Finally, implications of the DM model with respect to fracture, particularly crack extension and fracture toughness, are discussed.

PROPERTIES OF THE DM MODEL

Uniform internal tension

The DM model is illustrated in Fig. 1(a). It consists of a slit with an initial length $2c$ representing a crack in a semi-infinite plate of thickness t. Under the action of the nominal stress T, the slit extends to a length $2a$ and opens, but is partially constrained from extending and opening by a uniformly distributed internal tension of intensity S acting only on parts of the slit, from $x = \pm c$ to $x = \pm a$, and $\rho = (a - c)$.† Dugdale's basic argument is that if S is equated with Y (the yield strength of the material), the internal tension closely simulates the local support derived
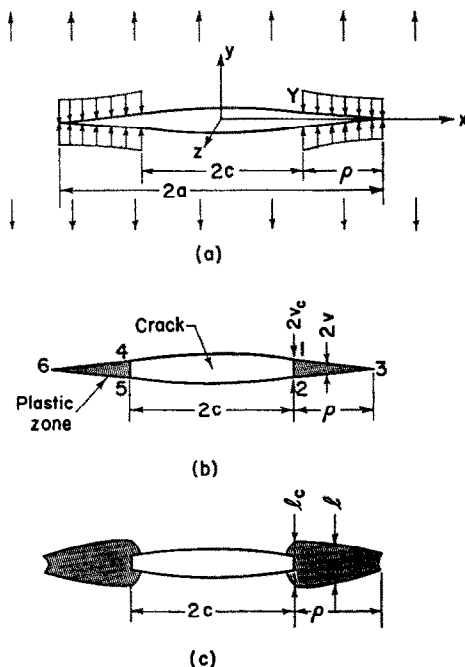

(a)

(b)

(c)

FIG. 1. Model of Dugdale–Muskhelishvili crack; (a) and (b) the DM model, (c) the actual crack.

---

† S is expressed as force per unit length corresponding to unit plate thickness. It is analogous to engineering stress, while Y is true stress.
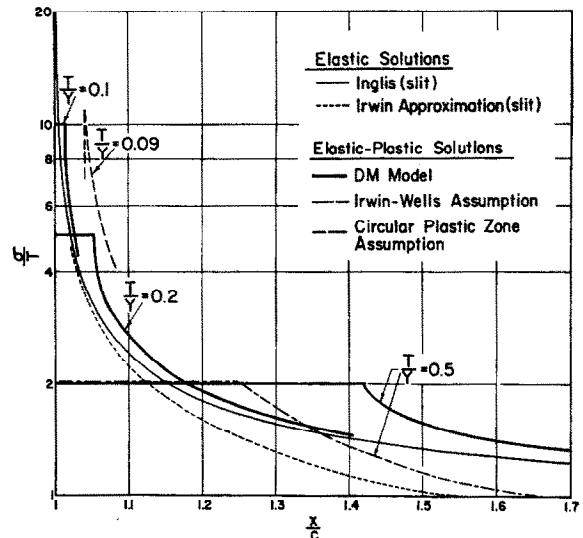

FIG. 2. Comparison of DM stress gradients with other solutions.

from similarly shaped wedges of yielded material, which are quite like zones observed experimentally (Fig. 1(c)). According to the Dugdale hypothesis, region 1245 (Fig. 1(b)) represents the partially relaxed crack, and regions 123 and 456 represent the attending plastic zones. Consistent with this idea, the plastic zones extend as long as the stress at points 3 and 6 (the elastic–plastic boundary) exceeds Y. By imposing this condition on the stress-field solution (see Appendix, Section 1), Dugdale was able to formulate the plastic-zone size in equilibrium with the applied stress:

$$\frac{\rho}{a} = 2\sin^2\frac{\beta}{2} \tag{1}$$

or

$$\frac{\rho}{c} = \sec\beta - 1 \tag{2}$$

where $\beta = \dfrac{\pi T}{2Y}$. The same relations have been derived for the case of a crack in pure shear[11] and torsion.[7]

Although Dugdale derived the stress-field solution (equation A-1), he did not publish the result or evaluate it numerically. We programmed this equation for a computer and found that the stress gradient for a wide range of applied stress levels is described by the equation (see Appendix, Section 2),

$$\sigma_{\substack{(y=0) \\ (x>a)}} = T + \frac{T}{\beta}\arctan\left(\frac{\sin 2\beta}{e^{2\alpha} - \cos 2\beta}\right), \tag{3}$$

where σ is the stress in the y direction, $\beta = \pi T/2Y$, and $\alpha = \mathrm{arc\ cosh}\ x/a$. Specific gradients are illustrated in Fig. 2. The DM plastic zone extends farther
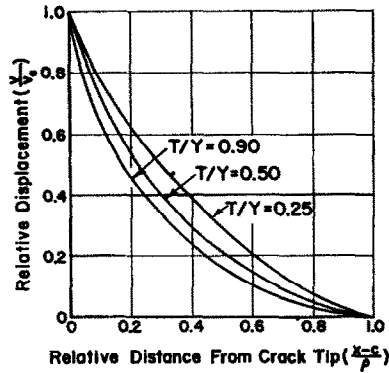
FIG. 3. Normalized displacement–distance curves for the DM model.[1-3,15]

than the zone derived from the Irwin[2] and Wells[3] assumptions, and about twice as far as the value given by the Inglis elastic solution (the $(x - c)/c$ value corresponding to Y). It is one-fourth the size of a completely relaxed circular plastic zone.[15] The DM elastic-stress-field is perturbed (relative to the elastic solutions) a distance 2ρ in front of the crack. Beyond a distance 2ρ, the DM and Inglis solutions converge. The DM model gives the steepest stress gradient near the plastic zone, approaching infinity as $x \to a$. It would appear that material just ahead of a moving crack is subjected to stress rates approaching shock loading.

The on-load displacement of a point on the slit wall (see Fig. 1(b)) has been worked out by Goodier and Field[14] for the DM model,

$$v = \frac{aY}{\pi E}\left(\cos\theta\ln\frac{\sin^2(\beta - \theta)}{\sin^2(\beta + \theta)}\right.$$
$$\left. + \cos\beta\ln\frac{(\sin\beta + \sin\theta)^2}{(\sin\beta - \sin\theta)^2}\right) \quad (4)$$

where v is the displacement in the y direction, E is Young's modulus, $\theta = \arccos x/a$, and Poisson's ratio is taken as $1/3$. Figure 3 shows that normalized displacement–distance curves for three widely separated values of T/Y are similar. Goodier and Field[14] also derived an expression for the displacement at the crack tip (Fig. 1(b)),

$$v_c = \frac{4Yc}{\pi E}\ln\sec\beta, \quad (5)$$

where $v_c \equiv v_{(x=c)}$. Equation (5), presented graphically in Fig. 4, is almost identical to the analogous expression derived by Bilby et al.,[11] for the case of shear. At low stresses $(T/Y \leqslant 0.6)$, equation (5) reduces to

$$v_c = \frac{\pi c T^2}{2EY} \quad (6)$$

In principle, the operation of the model can also be reversed to simulate unloading. When the load is removed, the opened slit tends to contract and close in response to the internal restoring stress field. But this is now opposed by the enlarged yielded region resisting with a pressure, $-Y$, acting on the crack walls from $c < x < a$. Under these conditions, the slit contracts as long as the stress at $x = \pm a$ exceeds $|Y|$.

As a useful approximation valid in the vicinity of the crack tip, the restoring stress field can be replaced by a uniform applied stress $-T_R$, such that T_R will produce in an unconstrained slit (i.e. $S = 0$) of length $2a$ the on-load value of v_c given by equation (5). As shown in Appendix, Section 3,

$$\frac{T_R}{Y} = \frac{2}{\pi}\cot\beta\ln\sec\beta \quad (7)$$

The effect of superpositioning T_R on T is equivalent to a tension $(T - T_R)$ acting on a virgin slit, $2c$, and this then describes the off-load state in the vicinity of the crack tip:

$$\frac{v_c'}{v_c} = \frac{\ln\sec\beta'}{\ln\sec\beta} \quad (8)$$

where v_c' is the off-load crack-tip displacement, and $\beta' = \pi(T - T_R)/2Y$. Values of v_c' and the ratio
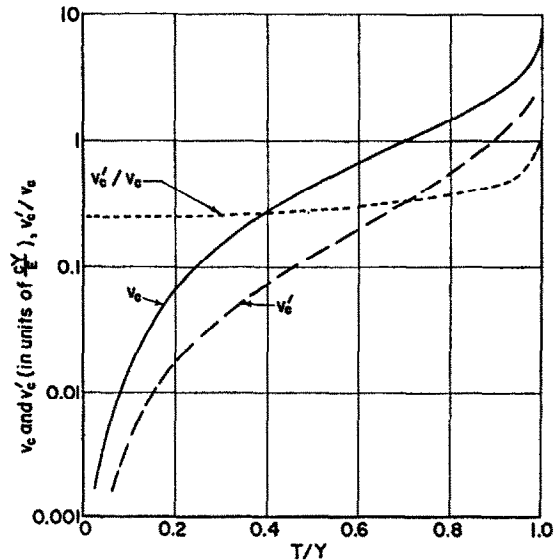

FIG. 4. Influence of stress level on v_c and v_c' the on-load and off-load cracktip displacement and the ratio v_c'/v_c.

v_c'/v_c calculated in this way are reproduced in Fig. 4. The results indicate that v_c'/v_c approaches 0.25 at low stress and 1 at high stress but is relatively invariant (e.g. 0.25–0.40) in the range $T/Y = 0$–0.85.

Nonuniform internal tension

The calculations outlined so far are valid for a uniform internal tension S (see Fig. 5(a)). This is not an unreasonable model for metals provided v_c is small and the rate of strain hardening is not an important factor. Otherwise, corrections must be applied for (1) the reduction in sheet thickness consistent with plastic deformation at constant volume† and (2) strain
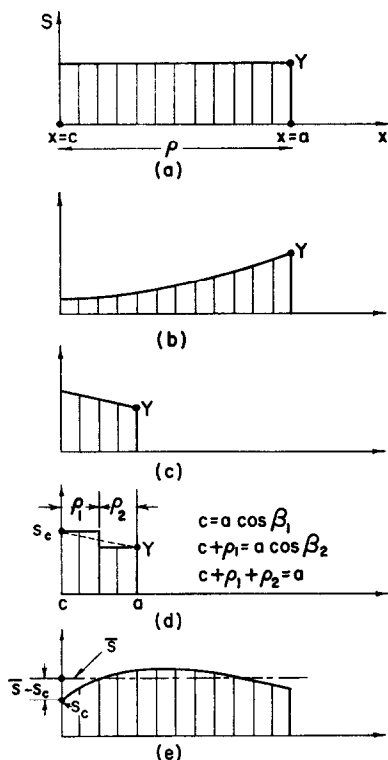

FIG. 5. Examples of different distributions of the internal tension, S.

hardening. For example, if deformation is confined to shear on a single 45° slip plane, displacements in the y direction must be accompanied by a reduction in the load-bearing cross section of the sheet given by $2v$. Consequently, if Y', defined as the true flow stress, is constant (e.g. $Y' = Y$), the internal tension S, opposing the opening of the crack, must diminish from a maximum value Y at $x = a$,

$$S(x) = Y \left[1 - \frac{2v(x)}{t} \right] \quad (9)$$

---

† In considering displacements and strains, the following simplifying assumptions consistent with constant volume deformation and the DM model are made:

$$\varepsilon = \varepsilon_y = \varepsilon_z, \varepsilon_x = 0; \quad v = v_y = v_z, v_x = 0;$$

$$v_y = \int_0^\infty \varepsilon_v(y) \, dy = \int_0^\infty \varepsilon_z(y) \, dy.$$

This is shown schematically in Fig. 5(b). If the material also strain hardens, then: (1) $Y' = Y'(\varepsilon)$ where ε is the strain and (2) the displacement is distributed over a finite volume—a spectrum of strains is now encountered. The reduction in the load-bearing cross section is $(1 - \varepsilon)$, and the maximum reduction (at $y = 0$) corresponds to the maximum strain ε^*,

$$S(x) = Y'(\varepsilon^*)[1 - \varepsilon^*] \quad (10)$$

Several points, therefore, emerge about the variable-internal-stress case:

(i) To establish $S(x)$, the distribution of strain, $\varepsilon(y)$, must be known. The model can only provide displacements; strains must be inferred from other considerations or measured experimentally. For example, the displacement can be expressed in terms of l the width of the plastic zone, and $\bar{\varepsilon}$ the average strain:

$$2v = l\bar{\varepsilon} \quad (11)$$

Experiments to be described indicate $l \sim t$. Since $\bar{\varepsilon} \sim \varepsilon^*/2$,

$$v \sim \frac{t\varepsilon^*}{4} \quad (12)$$

to a first approximation, and since v and x are related by an equation analogous to equation (4),

$$S(x) \sim Y'(v) \left[1 - \frac{4v}{t} \right] \quad (13)$$

If the internal stress distribution can be defined, then, as shown in Appendix, Section 4, the corresponding ρ, $\sigma(x)$, and $v(x)$ can be calculated.

(ii) Equations (10) and (13) show that the form of $S(x)$ is similar to a load elongation curve. Since strain hardening and the variation of v with x are essentially parabolic, the initial part of $S(x)$ is linear (see Fig. 5(c)). A two-step function (see Fig. 5(d)) is thus a convenient approximation of small yielded zones. This approximation, together with equation (13), was used to estimate the influence of work hardening on plastic-zone size for silicon steel (see Appendix, Section 5). The results, presented graphically in Fig. 6, indicate that the influence of strain hardening becomes significant for long cracks and high stress levels.

Another simple approximation, which takes into account the effect of work hardening on v_c', is to modify the definition of β' in equation (8) by replacing Y with $S_c \equiv S_{(x=c)}$, the flow stress corresponding to the maximum strain at the crack tip. This simple approximation neglects the Bauschinger effect.

The form of $S(x)$ at high stress levels is illustrated in Fig. 5(e). In this case, the instantaneous average $\bar{S}$
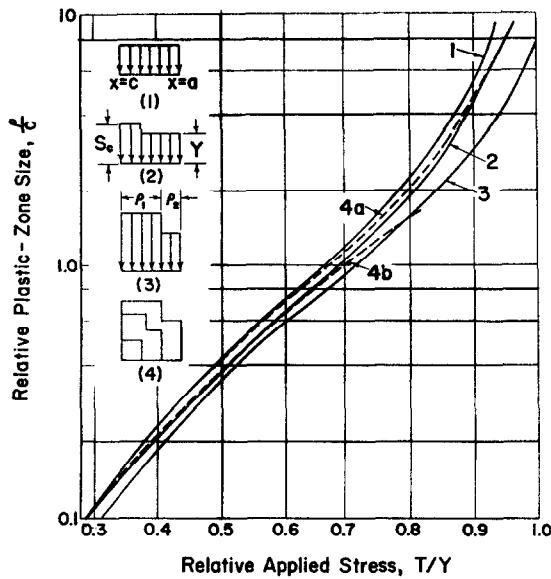
FIG. 6. Effect of work hardening on the relation between applied stress and plastic zone size. (1) Uniformly distributed internal tension; (2) two-step distribution $(S_c/Y = 1.20, \rho_1 = 0.5\rho_2)$; (3) two-step distribution $(S_c/Y = 1.33, \rho_1 - 2.0 \rho_2)$; (4) varying distribution simultating work hardening, (a) $c/t = 6.25$, (b) $c/t = 25.0$.

can serve as a useful approximation of the distribution, e.g. equation (2),

$$\frac{\rho}{c} = \sec\frac{\pi T}{2\bar{S}} - 1$$

where

$$\bar{S} \approx \frac{U + F}{2} \qquad (14)$$

and U and F are the ultimate tensile strength and fracture strength, both expressed in terms of engineering stress.

(iii) The shape of the plastic zone consistent with the mechanism of deformation will not necessarily correspond with the shape prescribed by the DM model. This could be taken into account by modifying the geometry of the DM model—replacing the slit by some other shape—but the refinement may not warrant the added complications.

The main problem, to be resolved by experiments, is the extent to which approximations inherent in the DM model impair the accuracy of its predictions. Dugdale[12] has already shown that the model gives a reasonable picture of the plastic-zone size in mild steel. The experiments described in the next two sections show that measurements of plastic-zone size and crack-tip displacements for silicon steel are also in accord with the theory.

EXPERIMENTAL PROCEDURE

Studies of locally yielded zones were carried out on large notched test coupons fabricated from 3% silicon steel (Si 3.31, C 0.04). The coupons (overall length 8 in., with a 4 × 2.5 in. gage section, and with centrally located edge slots 0.25 in. deep and 0.006 in. wide), derived from ¼-in. thick plate previously warm rolled 40% and stress relieved, were machined to thicknesses from 0.232 to 0.017 in. After machining, the coupons were recrystallized at 875° C and slowly cooled. The test specimens were loaded to various stress levels, held at maximum load for about 5 sec, unloaded, and later aged for 20 min at 150° C to decorate the dislocations. The stress–strain characteristics of this material in the annealed condition are shown in Fig. A1. The shape of the stress–strain curve is similar to that of a mild structural steel, but the strength level is higher, the lower yield stress $Y = 62{,}400$ psi. A complete summary of tests performed is given in Table 1.

Two different techniques were employed to reveal the plastic zone and the strain distribution within the zone. The off-load transverse strain field was photographed on an interference microscope. The interference pattern with isostrain contours and the corresponding strain profile for Sample S-56 are shown

TABLE 1. Summary of notch tests performed

Specimen number	Thickness, (in.)	T/Y	Zone type	ρ–Measured (in.)	ρ–Calculated‡ (in.)	ρ–Calculated§ (in.)
S-57	0.200	0.52	Hinge‖	$\rho^H \| = 0.072$	0.12	—
S-60	0.195	0.81	Transition	$\rho^H = 0.54 \quad \rho = 0.28$	0.58	0.40
S-58	0.232	0.90	45°-Shear	$\rho^H > 1.40\dagger \quad \rho = 0.60$	1.35	1.20
S-47	0.165	0.75	Transition			
S-48	0.128	0.90	45°-Shear			
S-53	0.060	0.78	45°-Shear	$\rho = 0.38$	0.48	0.44
S-55	0.017	0.52	45°-Shear	$\rho = 0.10$	0.12	0.10
S-56	0.017	0.81	45°-Shear	$\rho = 0.39$	0.58	0.40

† Although, in this sample, yielding was predominantly of the 45°-shear type, traces of plastic deformation of a hinge character were observed to the distance indicated.
‡ Calculated from equation (1) assuming no work hardening.
§ Calculated taking work hardening into account (Fig. 6 and Appendix, Section 5).
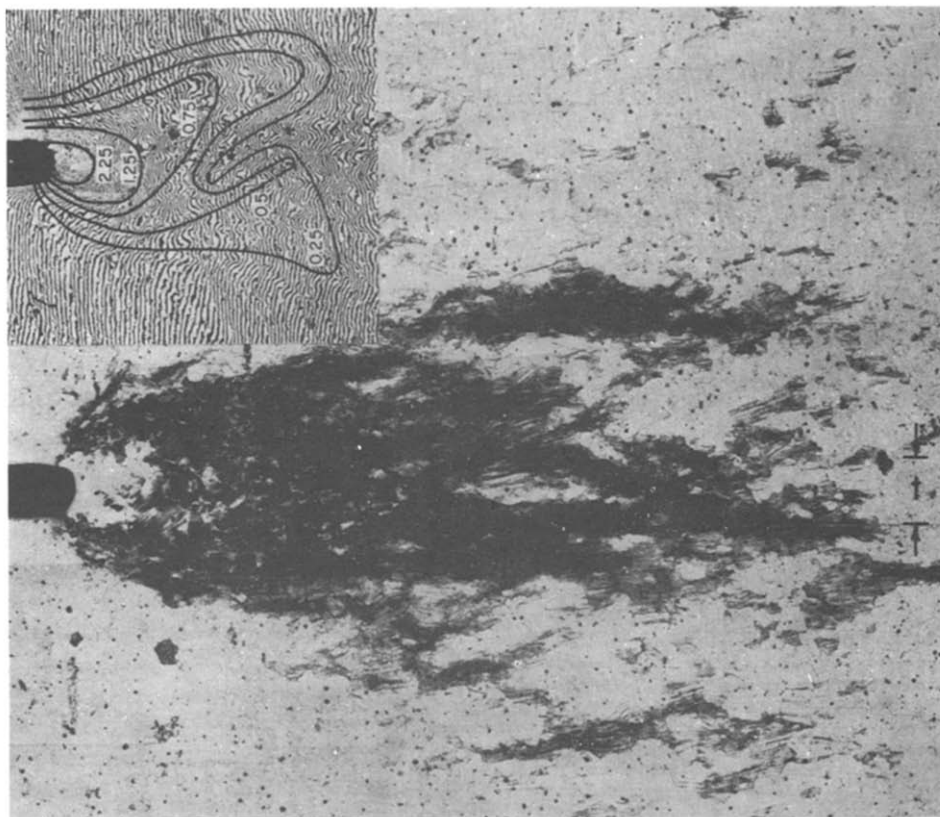‖ See Fig. 11 for definition of ρ^H.

FIG. 7. Interference pattern with isostrain contours (top left corner) and the corresponding plastic zone revealed by etching, both for Sample S-56 ($t = 0.017$ in., $T/Y = 0.81$). $\times 17.5$.
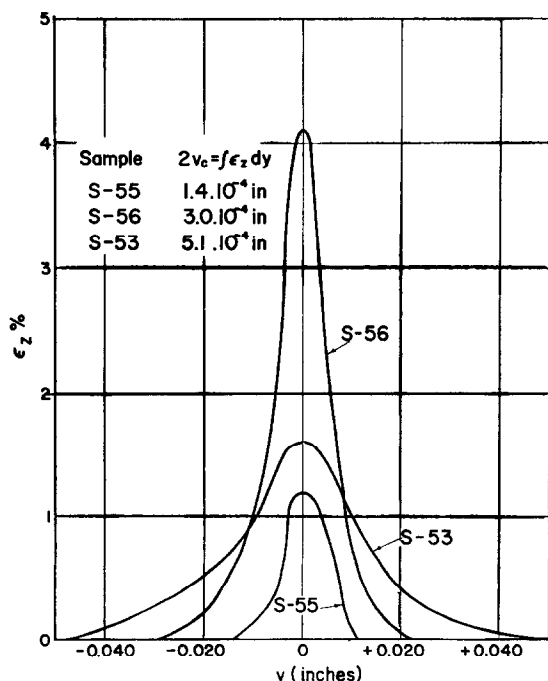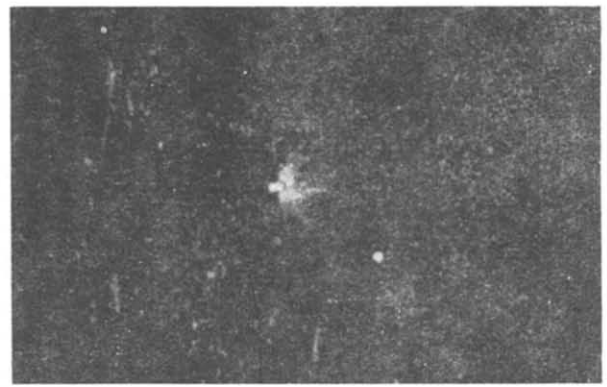

FIG. 8. Crack-tip strain profiles determined from interferometric measurement.

in Figs. 7 and 8. The strain profile was used to calculate v' $\left(v' = \int_0^\infty \varepsilon_z \, dy \right)$.
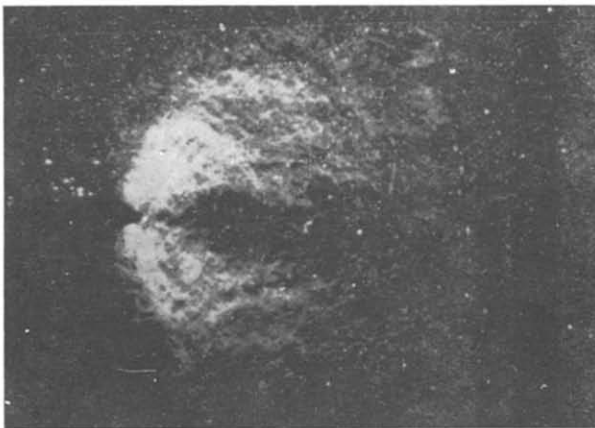
Following this, the surfaces of the test pieces were electropolished and etched, utilizing the Morris procedure,[16] to reveal the plastic zone, and then were reground to various depths, polished, and re-etched to delineate the zone on various interior sections. This method of etching, based on the preferential attack of individual dislocations, results in a gradual darkening of the surface as the strain increases to 1–2%. Beyond 2% strain the etching response diminishes, and above about 5% strain the material studied here was not attacked, probably because decoration was incomplete. Consequently, the technique revealed both the extent of the plastic zone and, to some degree, the distribution of strain within the zone. The change in etching response is illustrated in Fig. 7 which shows a highly strained but unetched region close to the notch tip. A displacement v_e can be calculated from l_e, the width of the etched region, and $\bar{\varepsilon}_e$, an average strain, deduced from the etching response, see equation (11). Since $v_e = v + (v - v')$,
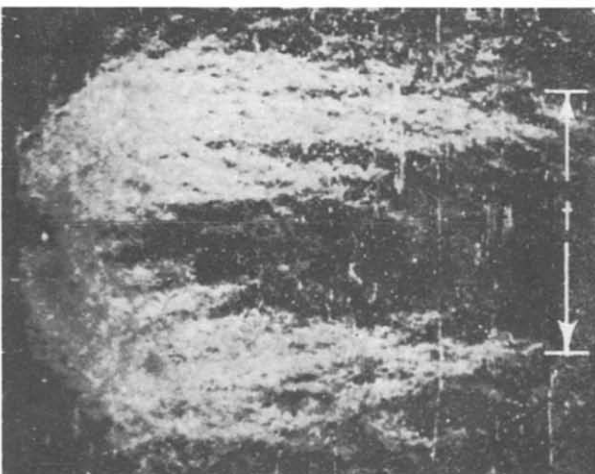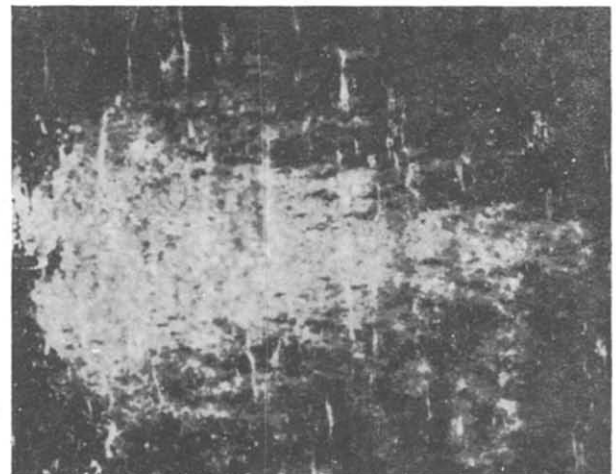
(a)

(b)

(c)

(d)

(e)

(f)

FIG. 9. Plastic zones revealed by etching the surface and midsection of notched coupons:
(a) and (b) Sample S-57 ($t = 0.200$ in., $T/Y = 0.52$)   (c) and (d) Sample S-60 ($t = 0.195$ in., $T/Y = 0.81$)
(e) and (f) Sample S-58 ($t = 0.232$ in., $T/Y = 0.90$)
Oblique illumination. ×6.08.

the sum of absolute values of displacement incurred when the load is applied plus the reverse displacement produced by unloading, it can be combined with v' from the interferometric measurement to give v, the on-load displacement,

$$v = \frac{v_e + v'}{2} \qquad (15)$$

EXPERIMENTAL RESULTS

The interpretation of plastic zones revealed by etching is complicated by the fact that yielding concurrent with loading is superimposed on reverse flow during unloading. Still, a reasonable picture emerges of the effect of stress and plate thickness on the character of the plastic zone. Three types of plastic zones are observed (see Figs. 7, 9, and 10):

1. Hinge-type zone. At low-stress levels the zone extends normal to the plane of the crack, and its form is essentially the same on all interior sections (see Figs. 9(a and b)). The shape of the zone is consistent with the idea that yielding occurs essentially by flow about hypothetical plastic hinges[17] (see Fig. 11). The hinge-type zone is also qualitatively in accord with Jacobs zone-shape calculations for plane strain.[5]

2. 45° shear type zone. At high-stress levels the zone is projected in front of the crack in the direction parallel to the crack plane. As shown in Figs. 7(b), 9(e, f), 10(d, e), this form bears a striking resemblance to the DM model. Etching the interior sections reveals that the mechanism of yielding in this case is shear on slabs inclined ~45° to the tensile axis, similar to necking of unnotched sheet coupons (see Fig. 11). As a consequence of the 45°-shear nature of the yielding, the zone width on the surface is approximately equal to the plate thickness; this is shown in Figs. 10(e) and 11(c).

3. Transition zone. At intermediate stresses, the zone appears in a state of transition between the hinge type and the 45°-shear type (see Figs. 9(c, d), 10(a, b)).

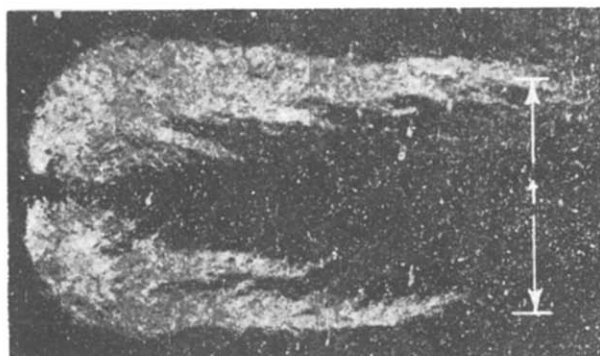Measurements of the zone size (summarized in Table 1) are in accord with previous experience. Consistent with Tetelman,[18] ρ^H (see Fig. 11) for the

(a)

(b)

(c)

(d)

FIG. 10. Plastic zones revealed by etching the surface and the midsection of notched coupons: (a) and (b) Sample S-47 ($t = 0.165$ in., $T/Y = 0.75$)   (c) and (d) Sample S-48 ($t = 0.128$ in., $T/Y = 0.90$) Oblique illumination. ×9.5.

TABLE 2. Comparison of measured crack-tip displacement values with predictions of the DM model

Sample number	T/Y	Derived from measurements†					Calculated		
		l_{ce} (in.)	$\bar{\varepsilon}_{ce}$ %	v_{ce} (10^{-4} in.)	v_c' (10^{-4} in.)	v_c (10^{-4} in.)	v_c'‡ (10^{-4} in.)	v_c§ (10^{-4} in.)	v_c‖ (10^{-4} in.)
S-55	0.52	0.026	3–4	4–6	0.7	2–3	0.8	0.9	2.5
S-56	0.81	0.044	4–7	10–14	3.4	6–9	3.1	3.7	8.1
S-53	0.78	0.063	3–4	18–24	2.1	6–7	2.6	3.1	7.0

† The quantities l_{ce}, $\bar{\varepsilon}_{ce}$, and v_{ce} are the average width, strain, and displacement, respectively, immediately in front of the slot as revealed by etching. $v_{ce} = \frac{1}{2}l_{ce}\bar{\varepsilon}_{ce}$. v_c' is derived from the interference pattern as described in the text. v_c is calculated from v_{ce} and v_c' via equation (15).

‡ Calculated from equations (7) and (8) using: $Y = 62{,}400$ psi, $E = 30{,}000{,}000$ psi, and $c = 0.250$ in.

§ These values of the off-load displacement were calculated taking work hardening into account as described in paragraph (ii) on p. 287 and p. 288.

‖ Calculated from equation (5).

hinge-type zone of Sample S-57 is described by

$$\frac{\rho^H}{c} \sim \frac{1}{2}\left(\sec\frac{\pi T}{2Y} - 1\right) \quad (16)$$

The extent of the 45°-shear-type zone of Sample S-55 is in good agreement with equation (2). Values for Samples S-56, S-63, S-48, and S-58 are somewhat smaller than predicted. Although better agreement is obtained when work hardening is taken into account (see Table 1), a discrepancy remains. This could be related to departures from the infinite plate solution (likely when the plastic zone covers more than 20–30% of the sample cross-section area) and to the fact that the DM model only approximates the shape of real zones.

The results summarized in Table 2 represent the first attempt to check displacement values predicted by the DM model. As shown, both the onload and off-load crack-tip displacement values derived from the etching response and the interferometric measurements are in reasonable accord with the theory. Work-hardening corrections do not improve the agreement in v'_c values for Samples S-53 and S-55; in both cases the maximum strain is small, and the Bauschinger effect could be more important than strain hardening.

On the basis of these results, it appears that the DM model offers a useful description of (a) shape, (b) size, and (c) displacements of a 45°-shear-type plastic zone. Two points bearing on the general applicability of the model should be kept in mind:

(i) First, the state of stress must be substantially plane stress. The 45°-shear mode will be constrained until the stress acting on regions a distance $t/2$ above and below the crack centerline, $y = 0$ (see Fig. 11), exceeds the yield stress. Yielding at this distance first becomes possible when

$$\rho^H > \frac{t}{2} \quad (17)$$

and this condition should approximately mark the beginning of the transition from the hinge-type to the 45°-shear-type zone. The configuration begins to approach a narrow, tapered DM-model zone when

$$\rho \sim 4t \quad (18)$$

since the zone width is $\sim t$. Limiting conditions for the various types of zones, formulated by combining equations (18) with (2) and (16) with (17), are summarized in Table 3. These conditions are consistent with the experimental observations.

(ii) The 45°-shear zone has, so far, only been observed in steel. In fact, the Stimpson and Eaton[6] theoretical calculations for plane stress do not predict a 45°-shear zone, but a shape with much more "hinge" character. Even when the bulk of the deformation is of the 45°-shear type, the silicon steel exhibits traces of deformation at distances $y > t/2$ (see Fig. 7
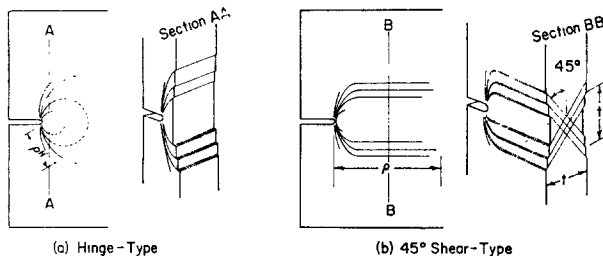

(a) Hinge-Type   (b) 45° Shear-Type

FIG. 11. Schematic drawing of the type of deformation associated with (a) the hinge-type and (b) the 45°-shear-type plastic zone.

TABLE 3. Limiting conditions for zone occurrence

Condition	Dominant zone
$\dfrac{t}{c} > \left(\sec\dfrac{\pi T}{2Y} - 1\right)$	Hinge type
$\left(\sec\dfrac{\pi T}{2Y} - 1\right) > \dfrac{t}{c} > \dfrac{1}{4}\left(\sec\dfrac{\pi T}{2Y} - 1\right)$	Transition
$\dfrac{t}{c} < \dfrac{1}{4}\left(\sec\dfrac{\pi T}{2Y} - 1\right)$	45°-shear type

and ρ^H for Samples S-60 and S-58 in Table 1), in keeping with the calculations.

The discrepancy between the Stimpson and Eaton calculations and the behavior of steel may be related to the choice of yield criterion (von Mises, as opposed to Tresca, in the case of the DM model), or to the yield point effect.[19] Until this point is resolved, the safest assumption is that the 45°-shear-type zone is one of several modes of relaxation possible under plane stress.

IMPLICATIONS FOR FRACTURE

Since it is both quantitatively meaningful and simple to handle, the DM model is especially useful in dealing with fracture. It can approximate the stress–strain-rate environment in front of a propagating crack.[15] It may have application to fatigue, since it can deal with loading and unloading. Finally, the DM model can be used to treat crack extension. In this case, the predictions of the model complement accepted theory and experiment and for this reason are outlined below.

Equation (6), for the crack-tip displacement when $T/Y < 0.6$, can be written

$$T = \left(\frac{2v_c YE}{\pi c}\right)^{1/2} \qquad (19)$$

and, in this form, compared with Irwin's basic condition for crack extension,

$$T^* = \frac{K_c}{(\pi c)^{1/2}} \qquad (20)$$

In this case, T^* is the critical stress for crack extension, and K_c (the fracture toughness) is an empirical measure of the material's resistance to cracking.[20]

The fact that equations (19) and (20) have the same form implies that K_c is related to v_c and can be calculated directly,

$$K_c = (2v_c^* YE)^{1/2} \qquad (21)$$

where v_c^* represents the crack-tip displacement at crack extension.

The connection between v_c^* and K_c was first recognized by Wells,[21] and an expression similar to equation (21) has been derived by Bilby et al.[11]

Since K_c and Y are material constants, the quantity v_c^* must also be constant. The constancy of v_c^* can be related to invariance on the part of ε_c^*, a critical maximum crack-tip strain, via equations (11) and (12). Two mechanisms of crack extension can be related to a specific strain level:

1. Ductile fracture. Ductile fracture by the process of voids coalescing[22] might be expected to occur just in front of the crack tip when the maximum strain at this point reaches a level comparable to the reduction in area of an unnotched coupon.

$$\varepsilon_c^* = RA \qquad (22)$$

The crack then grows a small increment, and the maximum strain must increase further $\left(\dfrac{\partial \varepsilon_c^*}{\partial_c}\right)_{T,Y} > 0$, see equations (5) and (12). Since the strain at the crack tip is already beyond the capabilities of the material, an instability is inevitable. Locally, the origin of such failures is ductile fracture, but they are frequently classified as brittle when the failure stress is below the stress level for general yielding.

As shown in Table 4, K_c values, calculated directly from equations (12), (21) and (22), for 4330 steel and

TABLE 4. Comparison of measured and predicted values of the fracture toughness K_c and gross failure stress T^*

Material	Critical crack length, (inch)	K_c, (ksi $\sqrt{}$ in.)		T^*, (psi)	
		Measured[23]	Calculated §	Measured[23]	Calculated ‖
		A. Low stress levels, $T/\bar{S} < 0.7$ ¶			
4330†	2–10	300	420		
2219-T87‡	5–13	110	99		
		B. High stress levels, $T/\bar{S} > 0.7$ ¶			
4330†	0.5			190,000	200,000
2219-T87‡	0.8			57,000	58,000
2219-T87‡	1.4			49,000	53,000

† 4330 steel data:[23]
   $t = 0.140$ in., $E = 30,000,000$ psi, $Y = 189,000$ psi, $U = 223,000$ psi, $\bar{S} = 206,000$ psi, $F = 178,000$ psi, $RA = 45\%$, $\varepsilon_u = 6\%$.
‡ 2219-T87 aluminum data:[23]
   $t = 0.100$ in., $E = 11,000,000$ psi, $Y = 59,000$ psi, $U = 69,000$ psi, $\bar{S} = 64,000$ psi, $F = 56,000$ psi, $RA = 30\%$, $\varepsilon_u = 7\%$.
§ Equations (12), (21) and (22).
‖ Equations (12), (23) and (24).
¶ $\bar{S} = \dfrac{Y + U}{2}$.

2219-T87 aluminum are reasonably consistent with experiment,[23] considering the approximations made. If the relation between $v_c{}^*$ and $\varepsilon_c{}^*$ were known more precisely, even better agreement might be obtained.

2. *Plastic instability.* Another possibility is that the plastic zone become unstable first, and that ductile fracture (and crack extension) follows in the wake of the instability. This idea, which was recently proposed by Krafft,[24] can be formulated using the DM model. As shown in the Appendix, Section 6, the instability condition is approximately

$$\left(\frac{\bar{S} - S_c}{\bar{S}}\right) >$$

$$\left(\sec \frac{\pi T}{2\bar{S}} - 1\right)\left[\left(\frac{\pi T}{2\bar{S}}\right)\left(\sec \frac{\pi T}{2\bar{S}}\right)\left(\tan \frac{\pi T}{2\bar{S}}\right)\right]^{-1} \quad (23)$$

Figure 12, a plot of the criterion of equation (23), shows that considerable unloading is tolerated at low stress levels (e.g. $T/\bar{S} < 0.7$), but the plastic zone becomes unstable as a result of a small decrease in S_c when the stress is high (e.g. $T/\bar{S} > 0.7$). Consequently, plastic instability is the more likely mechanism of crack extension at high stress if the material is reasonably ductile.

According to this picture, $v_c{}^*$ and $\varepsilon_c{}^*$ associated with plastic instability (and failure) decrease as the stress is raised. Since equation (21) is not valid at high stresses, a simple relation among K_c, T^*, and c cannot be derived. However, the value of $\varepsilon_c{}^*$ at instability can be estimated (see Appendix, Section 6),

$$\varepsilon_c{}^* \approx \varepsilon_u + \sqrt{H\left(\frac{\bar{S} - S_c}{\bar{S}}\right)} \quad (24)$$

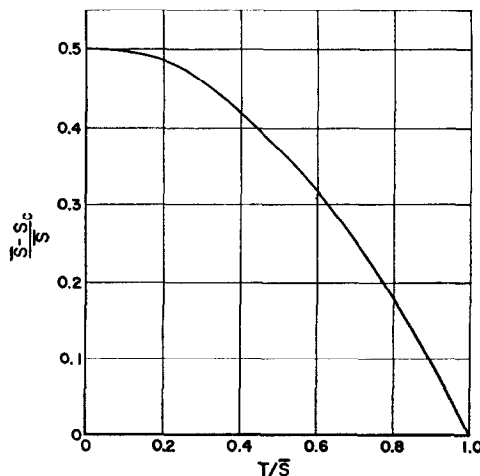where $H = (\varepsilon_f - \varepsilon_u)^2\left(\frac{U - F}{U}\right)^{-1}$, and U and F

FIG. 12. Criterion for plastic instability of a DM zone.

are the ultimate tensile stress and fracture stress (engineering stress), and ε_u and ε_f are the corresponding strains (expressed as reduction in area). Equations (24), (12) and (23) together fix the value of T at instability. As shown in Table 4, failure stress values calculated in this way are in good accord with actual measurements and consistent with the apparent decrease of K_c observed at high stress levels, i.e. $T/Y > 0.8$.[23]

CONCLUSIONS

1. For edge-slotted silicon steel, local yielding is predominantly of the plane strain *plastic-hinge* type until the extent of the yielded zone is about equal to the sheet thickness. Further deformation, under plane stress conditions, proceeds by a *45°-shear* mode.

2. The general shape of the 45°-shear zone can approach that of the DM (Dugdale–Muskhelishvili) crack model. Predictions of this model are in agreement with measured zone size and displacement values for silicon steel.

3. The DM model offers a relatively simple expression of the stress gradient and can be used to estimate effects of work hardening and unloading. Calculations and experiments indicate that the off-load cracktip displacement approaches 25% of the on-load value at low stress.

4. The DM model can be used to formulate the conditions for crack extension. Failure stress values and the fracture toughness, K_c, calculated in this way from first principles, are in accord with experiment.

REFERENCES

1. C. E. INGLIS, *Trans. Instn. Nav. Archit.*, Lond. **55**, 219 (1913).
2. G. R. IRWIN, *J. Appl. Mech.* **24**, 361 (1957).
3. A. A. WELLS, *Brit. Weld. J.* **10**, 855 (1963).
4. D. N. DE G. ALLEN and R. V. SOUTHWELL, *Phil. Trans.* **A242**, 379 (1950).
5. J. A. JACOBS, *Phil. Mag.* **41**, 349 (1950).
6. L. D. STIMPSON and D. M. EATON, Technical Report ARL24, California Institute of Technology, 1961.
7. J. A. H. HULT and F. A. MCCLINTOCK, *9th Int. Cong. Appl. Mech.* **8**, 51 (1957).
8. F. A. MCCLINTOCK, *Mat. Res. Stand.* **1**, 277 (1961).
9. F. A. MCCLINTOCK, *Fracture of Solids* (Edited by DRUCKER and GILMAN) p. 65, Interscience, New York (1963).
10. J. F. KNOTT and A. H. COTTRELL, *J. Iron St. Inst.* **201**, 249 (1963).
11. B. A. BILBY, A. H. COTTRELL and K. H. SWINDEN, *Proc. Roy. Soc.* **A272**, 304 (1963).
12. D. S. DUGDALE, *J. Mech. Phys. Solids*, **8**, 100 (1960).
13. N. I. MUSKHELISHVILI, *Some Basic Problems of the Mathematical Theory of Elasticity*, p. 340, Noordhoff, Gronigen (1953).

14. J. N. GOODIER and F. A. FIELD, *Fracture of Solids* (Edited by DRUCKER and GILMAN) p. 103, Interscience, New York (1963).
15. G. T. HAHN, A. GILBERT and C. N. REID, *J. Iron St. Inst.* **202**, 677 (1964).
16. C. E. MORRIS, *Metal Progr.* **56**, 696 (1949).
17. A. P. GREEN and B. B. HUNDY, *J. Mech. Phys. Solids*, **4**, 128 (1956).
18. A. S. TETELMAN, *Acta Met.* **12**, 993 (1964).
19. J. L. SWEDLOW, California Institute of Technology; private communication, 1964.
20. G. R. IRWIN, *Metals Engineering Quarterly*, **3**, 24 (1963).
21. A. A. WELLS, *Proceedings of Crack Propagation Symposium*, 1961, sponsored by Roy. Aer. Soc., **1**, p. 210, published by College of Aeronautics, Cranfield, England (1962).
22. H. C. ROGERS, *Trans. Amer. Inst. Min. (Metall.) Engrs.* **218**, 498 (1960).
23. ASTM Committee on Fracture Testing of High Strength Materials, Materials Research & Standards, **4**, 107 (1964).
24. J. M. KRAFFT, *Appl. Mat. Res.* **3**, 88 (1964).

APPENDIX

1. Previous work

Using Muskhelishvili's[13] method, the normal stress, σ, in front of a slit subjected to the stress system shown in Fig. 1 is found to be

$$\sigma_{\substack{(y=0) \\ (x>a)}} = \left(T - \frac{2\beta Y}{\pi}\right) \coth \alpha$$

$$+ T\left\{1 - \frac{1}{\beta}\arctan\frac{\sin 2\beta}{\cos 2\beta - e^{2\alpha}} - \frac{Qe^{\alpha}}{4\beta}\right\} \quad (A1)$$

where T = applied stress, Y = yield stress, $\cos \beta = c/a$, $\cosh \alpha = x/a$,

$$Q = \frac{\delta_A' \cosh \alpha}{(\sinh \alpha)^3}(3[\sinh \alpha]^2 + \cosh \alpha \sinh \alpha - 1)$$

$$+ \delta_A'(\coth \alpha)^2\left[1 - \frac{\delta_A' e^{\alpha}(e^{2\alpha} - \cos 2\beta)}{\sin 2\beta}\right]$$

$$- \frac{\delta_B' \cos \beta}{(\sinh \alpha)^3}(3[\sinh \alpha]^2 + \cosh \alpha \sinh \alpha - [\cosh \alpha]^2)$$

$$- \frac{\delta_B' e^{\alpha} \cos \beta}{(\sinh \alpha)^2}\left[1 + \frac{\delta_B'(1 - e^{2\alpha} - 2[\sin \beta]^2)}{2\sin \beta}\right],$$

$$\delta_A' = \frac{4 \sin 2\beta\, e^{\alpha}}{(e^{2\alpha} - \cos 2\beta)^2 + (\sin 2\beta)^2},$$

and

$$\delta_B' = \frac{4 \sin \beta(1 + e^{2\alpha})}{(1 + e^{2\alpha})^2 - (2e^{\alpha}\cos \beta)^2}.$$

The other terms of equation (A1) are defined in Fig. 1. To avoid the infinity at $\alpha = 0$ ($x = a$), the coefficient of $\coth \alpha$ must vanish:

$$\beta = \frac{\pi}{2}\frac{T}{Y} = \text{arc cos } (c/a) \quad (A2)$$

2. Stress analysis for uniformly loaded slit

Equation (A1) was programmed for a digital computer and σ and Q determined for 792 combinations
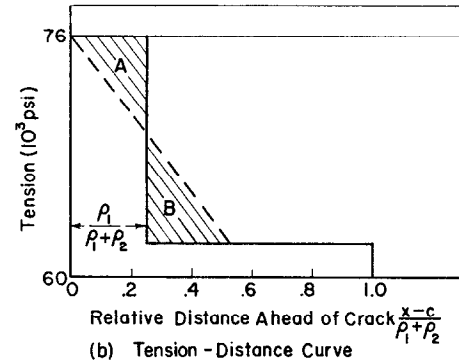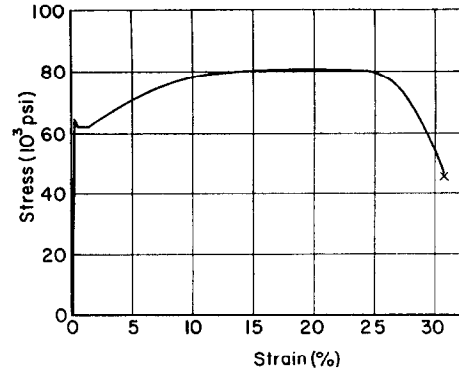

FIG. A1. Conversion of stress–strain curve into tension–distance curve.

of α and β. It was found that Q was negligibly small, except for values of α so small as to introduce rounding off errors in the computer ($x/a < 1.0002$ and $T/Y < 0.006$). It can also be shown by series approximations that Q approaches 0 as α approaches 0. We have concluded that Q can be ignored, and that

$$\frac{\sigma}{T} = 1 + \frac{1}{\beta}\arctan\left\{\frac{\sin 2\beta}{e^{2\alpha} - \cos 2\beta}\right\} \quad (A3)$$

3. Displacement

The displacement at any point on a slit under a uniform tension when the slit is not restrained by an internal stress is

$$v = \frac{(k + 1)aT \sin \theta}{4\mu} \quad (A4)$$

k is the function of Poisson's ratio, ν, where $k = (3 - \nu)/(1 + \nu)$ for plane stress. The displacement at a distance, c, from the center of such a slit is

$$v_c = \frac{(k + 1)cT \tan \beta}{4\mu} \quad (A5)$$

since $c/a = \cos \beta$, and $\theta = \beta$.

The displacement equations for the relaxed slit of the DM model have been calculated by Goodier and Field,[14] and are found in the body of the paper. In

particular, the critical displacement for an internally stressed slit (see Fig. 1(a)) is

$$v_c = \frac{(k+1)cY}{2\mu\pi} \ln \sec \beta \qquad \text{(A6)}$$

To determine the stress, T_r, producing the same displacement in a slit of the same length in the absence of an internal stress, (A6) is substituted into (A5)

$$\frac{T_R}{Y} = \frac{2}{\pi} \cot \beta \ln \sec \beta \qquad \text{(A7)}$$

4. Stress and plastic-zone size for arbitrarily loaded slit

Since all terms in the Muskhelishvili formulation which involve derivatives of δ_A and δ_B do not appear in equation (A3), expressions for a slit subjected to any arbitrary combination of internal and external loads can be derived easily. For example, the stress distribution in front of the slit of Fig. 5(d) can be found by the summation of three solutions ($\sigma = \sigma_1 + \sigma_2 + \sigma_3$):

(1)   External tensile stress, $\sigma_1 = T \coth \alpha$ (A8)

(2) Uniform internal pressure, $-S_c$, applied to the regions

$$|a| > |x| > |c| : \sigma_2 = \frac{-S_c}{\pi} \{2\beta_1[\coth \alpha - 1] + \delta_A(\beta_1)\}$$
$$\text{(A9)}$$

(3) Uniform internal pressure $(S_c - Y)$ applied to the regions

$$|a| > |x| > (|c| + |\rho_1|) : \sigma_3$$

$$= \frac{S_c - Y}{\pi} \{2\beta_2 [\coth \alpha - 1] + \delta_A(\beta_2)\} \quad \text{(A10)}$$

where $\delta_A = -2 \arctan \left(\frac{\sin 2\beta}{e^{2\alpha} - \cos 2\beta} \right)$

Setting the coefficient of $\coth \alpha$ equal to 0, results in the restriction,

$$\frac{\pi T}{2} = (\beta_1 - \beta_2)S_c + \beta_2 Y \qquad \text{(A11)}$$

and the solution

$$\frac{\sigma}{T} = 1 + \frac{\delta_A(\beta_2)}{\pi T} (S_c - Y) - \frac{\delta_A(\beta_1)S_c}{\pi T} \quad \text{(A12)}$$

Keeping the same boundary conditions ($S = S_c$ at $\beta = \beta_1$ and $S = Y$ at $\beta = 0$), but letting $S(\beta)$ now be an arbitrary function of β, equations (A8) and (A9) can be added to

$$\sigma_3 = \frac{1}{\pi} \int_{S_c}^{Y} \{2\beta[\coth \alpha - 1] + \delta_A(\beta)\} dS(\beta), \quad \text{(A10a)}$$

to give σ and the restriction,

$$\frac{\pi T}{2} = \beta_1 S_c + \int_{S_c}^{Y} \beta \, dS(\beta) \qquad \text{(A11a)}$$

The displacements for an arbitrarily loaded slit can be obtained by replacing Y in Equation (4) with

$$Y_c + \frac{1}{\beta_1} \int_{S_c}^{Y} \beta \, dS(\beta)$$

5. A method of simulating the effect of work hardening

Consider the material whose stress–strain curve is given by Fig. A1(a). Assume that ϵ_c, the strain at the crack tip, is 8%. For a given value of t (0.08 in.), the displacement at the crack tip can be calculated if it is assumed $v_c = \epsilon_c t/4 = 1.6 \times 10^{-3}$ in. For other points in the plastic zone, the displacement can be found from Fig. 3 and the relation $\epsilon/\epsilon_c = v/v_c$. Since each strain will correspond to a flow stress on Fig. A1(a), the tension–distance curve (Fig. A1(b)) can be calculated for a given T/Y. For ease in further computation, a two-step stress distribution, which simulates the calculated one is found by matching areas A and B (Fig. A1(b)) and the stress distribution in front of the plastic zone, the plastic-zone size, and displacements found by the method outlined in Section 4.

To determine the solid lines on Fig. 6, the displacements (v_c) corresponding to the various strains were calculated from equations (11) and (12) with $t = 0.08$ in. The two-step distribution was replaced by a uniform distribution and T/Y found from Fig. 4. Although each solid line was calculated for a specific crack length and sheet thickness, it applies to any specimen with the same c/t ratio (see equations (11) and (12) and (A6)). Plastic-zone sizes for $\frac{1}{4}$ in. cracks in thicknesses other than 0.08 in. were found by determining c/t and interpolating between the curves of Fig. 6.

6. Plastic-zone instability

If the applied stress is held constant, but the tension S (reflecting the yield stress of the material) is allowed to vary, the rate of change of the equilibrium zone size is given by

$$\left. \frac{\partial \ln \rho}{\partial \ln S} \right|_T =$$
$$-\left(\sec \frac{\pi T}{2S} - 1 \right)^{-1} \left(\frac{\pi T}{2S} \sec \frac{\pi T}{2S} \tan \frac{\pi T}{2S} \right) \quad \text{(A13)}$$

It is necessary to postulate a variable S when we consider a zone loaded with nonuniform tension distribution, $S(x)$, which is to be represented by a uniform

average tension $\bar{S} = 1/\rho \int_{c}^{(c+\rho)} S \, dx$ (see Fig. 5(e)). If the tension at the crack tip, S_c, changes, the corresponding change in plastic-zone size is easily seen to be

$$\frac{\partial \ln \rho}{\partial \ln \bar{S}} = \frac{-\bar{S}}{\bar{S} - S_c} \qquad (A14)$$

If the stress–strain curve is falling, i.e. $\partial S_c/\partial \rho < 0$, and $S_c < \bar{S}$, the rate of increase in plastic-zone size predicted from equation (A13) may be larger than can be tolerated by the conditions of equation (A14). Thus an instability results when

$$\frac{\bar{S} - S_c}{\bar{S}} > \left(\sec \frac{\pi T}{2\bar{S}} - 1\right)\left(\frac{\pi T}{2\bar{S}} \sec \frac{\pi T}{2\bar{S}} \tan \frac{\pi T}{2\bar{S}}\right)^{-1} \quad (A15)$$

The crack-tip strain at plastic instability can be estimated by noting that the relation between Y' (true stress) and ε^* (reduction in area) is approximately linear beyond the point of necking. Together with equation (10), this leads to a simple parabolic relation between ε^* and the tension S (S is equivalent to the engineering stress in a tensile test). The equation of the parabola with a vertex at U, ε_u, and passing through F, ε_f is

$$\varepsilon^* = \varepsilon_u + \sqrt{H\left(\frac{U - S}{U}\right)} \qquad (A16)$$

where $H = U(\varepsilon_f - \varepsilon_u)^2/(U - F)$, and U, ε_u, and F, ε_f are the engineering stress and strain at maximum load and fracture, respectively. The following approximation

$$\frac{\bar{S} - S}{\bar{S}} \approx \frac{U - S}{U} \qquad (A17)$$

is reasonable, particularly for high-strength materials exhibiting little work hardening. Consequently, the value of ε_c^* corresponding to a critical value of $\left(\dfrac{\bar{S} - S_c}{\bar{S}}\right)$ is

$$\varepsilon_c^* \approx \varepsilon_u + \sqrt{H\left(\frac{\bar{S} - S_c}{\bar{S}}\right)}. \qquad (A18)$$